10. Carbonate Dissolution Episodes in Paleocene and Eocene Sediment, Shatsky Rise, West-Central Pacific[1]

Haidi J.L. Hancock[2] and Gerald R. Dickens[3]

ABSTRACT

Holes 1209A and 1211A on Southern High, Shatsky Rise contain expanded, nearly continuous records of carbonate-rich sediment deposited in deep water of the equatorial Pacific Ocean during the Paleocene and Eocene. In this study, we document intervals of carbonate dissolution in these records by examining temporal changes in four parameters: carbonate content, coarse size fraction (>38 μm), benthic foraminiferal abundance, and planktonic foraminiferal fragmentation ratio. Carbonate content is not a sensitive indicator of carbonate dissolution in the studied sections, although rare intervals of low carbonate may reflect times of relatively high dissolution. The proportion of coarse size fraction does not accurately record carbonate dissolution either because the relative abundance of nannofossils largely determines the grain-size distribution. Benthic abundance and fragmentation covary ($r^2 = 0.77$) and are probably the best indicators for carbonate dissolution. For both holes, records of these parameters indicate two episodes of prominent dissolution. The first of these occurs in the upper Paleocene (~59–58 Ma) and the second in the middle to upper Eocene (~45–33.7 Ma). Other intervals of enhanced carbonate dissolution are located in the upper Paleocene (~56 Ma) and in the upper lower Eocene (~51 Ma). Enhanced preservation of planktonic foraminiferal assemblages marks the start of both the Paleocene and Eocene epochs.

[2]School of Earth Sciences, James Cook University, Townsville QLD 4811, Australia. **Haidi.Hancock@jcu.edu.au**
[3]Department of Earth Science, Rice University, Houston TX 77005, USA

INTRODUCTION

Calcite and aragonite produced by plankton sinks toward the seafloor throughout the oceans. At some depth, depending on mineralogy, this carbonate begins to dissolve because of unfavorable physiochemical conditions. The carbonate compensation depth (CCD) is the depth where carbonate dissolution exceeds carbonate supply so that no carbonate accumulates on the seafloor (Murray and Renard, 1891; Bramlette, 1961). The water column above the CCD where the preservation of carbonate decreases noticeably (often ~2 km in depth) is the lysocline (Berger, 1971). Early experiments evaluating the lysocline involved measuring weight loss in suspended calcite spheres (Peterson, 1966). When samples of foraminiferal ooze are suspended in the lysocline, thin-walled planktonic tests preferentially dissolve and shell fragmentation increases (Berger, 1967).

The CCD and lysocline at a given location may change over geological time in response to variations in carbonate supply and properties of deep ocean waters (e.g., Berger, 1974, 1992; Farrell and Prell, 1989; Le and Shackleton, 1992; LaMontagne et al., 1996). Stable oxygen and carbon isotope records constructed using benthic foraminifers display a series of large-amplitude excursions during the Paleocene and Eocene at ~65–33.7 Ma, especially spanning the late Paleocene, the Initial Eocene Thermal Maximum (IETM), and the Early Eocene Climatic Optimum (EECO) (Fig. F1). These perturbations in $\delta^{18}O$ and $\delta^{13}C$ of deep-sea carbonate are generally interpreted as representing profound changes in early Cenozoic deepwater temperatures and global carbon cycling. As such, they might also correspond to times of significant depth variation in the CCD and lysocline. Enhanced deep-sea carbonate dissolution clearly coincided with a prominent –3‰ excursion in the $\delta^{13}C$ of benthic foraminifers at the IETM (Kennett and Stott, 1991; Schmitz et al., 1996; Thomas and Shackleton, 1996; Zachos et al., 2001), both phenomena signifying a rapid, massive input of carbon to the ocean and atmosphere (Dickens et al., 1997; Dickens, 2000). For most intervals of the Paleocene and Eocene, however, established records of deep-sea carbonate dissolution (van Andel, 1975; Lyle, Wilson, Janacek, et al., 2002) are not sufficiently well constrained for correlation with isotopic perturbations and, by inference, episodes of global oceanographic change.

During Leg 198, a series of locations was cored on Shatsky Rise in the North Pacific (Fig. F2) to evaluate the record of Cretaceous and Paleogene oceanographic change (Shipboard Scientific Party, 2002). During the Paleocene and Eocene, the crest of Shatsky Rise was nominally at 1500 m water depth (Ito and Clift, 1998; Sager et al., 1999). The relatively thick and complete Paleogene sedimentary successions down the flanks of Shatsky Rise (Krasheninnikov, 1981; Sliter and Brown, 1993) should, therefore, hold a record of past fluctuations in carbonate dissolution. In this study, carbonate content, coarse size fraction, benthic foraminiferal abundance, and planktonic foraminiferal fragmentation were measured in samples of Paleocene and Eocene sediment from Holes 1209A and 1211A on the Southern High of Shatsky Rise (Fig. F2). Our primary aim was to document intervals of enhanced dissolution between 65 and 33.7 Ma. We also compare our records to the Paleogene CCD curve recently published for the equatorial Pacific Ocean (Lyle, Wilson, Janacek, et. al., 2002).

F1. Paleocene and Eocene geochronology, Hole 1211A, p. 13.
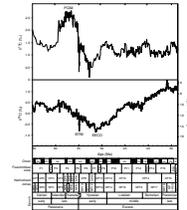
F2. Locations, Sites 1209 and 1211, p. 14.
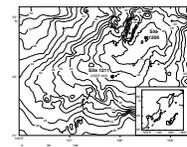
SITES AND SAMPLES

Shatsky Rise is a large igneous province in the northwest Pacific that rises from surrounding abyssal plains to a present-day water depth of 2000 m. This feature originally formed in the central equatorial Pacific at ~148 Ma and subsequently moved south and then northwest to its present-day position (Sager et al., 1999; Shipboard Scientific Party, 2002). During the Paleocene and Eocene, Shatsky Rise lay at ~20°N (Larson et al., 1992; Shipboard Scientific Party, 2002). Thermal subsidence models (Ito and Clift, 1998) and rudist fossils dredged from the south edge of the Southern High (Sager et al., 1999) indicate that Shatsky Rise was subaerially exposed during and immediately after eruption. During the Paleogene, however, Shatsky Rise submerged to water depths between 1500 and 4000 m (Ito and Clift, 1998; Sager et al., 1999). Importantly, Shatsky Rise received little siliceous material during the Paleocene and Eocene and has always been distant from a continental margin and associated terrigenous inputs (Bralower, Premoli Silva, Malone, et al., 2002). These factors simplify interpretations of the sedimentary record.

Eight sites were drilled on Shatsky Rise (Shipboard Scientific Party, 2002). Boreholes at two of these sites were chosen for this study. Site 1209 is located close to the top of the Southern High at 32°39.10′N, 158°30.36′E (2387 m water depth), and Site 1211 is located 100 km to the southwest on the southern flank of the Southern High at 32°00.13′N, 157°51.00′E (2907 m water depth) (Fig. F2). The two sites thus comprise a depth transect of 520 m. Site 1211 was drilled at the location of Deep Sea Drilling Project (DSDP) Site 305 (Larson, Moberly, et al., 1975). According to thermal subsidence curves (Ito and Clift, 1998), Site 305 (and, hence, Site 1211) lay beneath ~2.5 km of water during the Paleocene and Eocene. Site 1209 was under ~2.0 km of water during this time, assuming a similar depth offset between Sites 1209 and 1211 throughout the Cenozoic. The CCD in the equatorial Pacific was probably between 3 and 4 km for good portions of the Paleocene and Eocene (van Andel, 1975; Lyle, Wilson, Janacek, et al., 2002). Sites 1209 and 1211 should, therefore, be ideal locations to monitor fluctuations in the early Paleogene lysocline.

Three holes were cored at each of Sites 1209 and 1211. These holes extend to ~320 meters below seafloor (mbsf) at Site 1209, and ~180 mbsf at Site 1211 (Shipboard Scientific Party, 2002). By splicing together sections from the holes, composite logs were constructed for both sites (Shipboard Scientific Party, 2002). Depths on these logs and in this study are thus reported in meters composite depth (mcd). Apparently continuous Paleocene and Eocene sections occur from ~140 to 255 mcd at Site 1209 and from ~85 to 150 mcd at Site 1211 (Shipboard Scientific Party, 2002) (Fig. F3). Paleocene and Eocene sediments at both sites are primarily very pale orange nannofossil and moderate yellowish brown clayey nannofossil ooze, commonly showing decimeter- to meter-scale cyclicity. Interestingly, this cyclicity is more pronounced at the shallower Site 1209. Paleocene and Eocene sediments at Sites 1209 and 1211 were dated using planktonic foraminiferal assemblages (M.R. Petrizzo, pers. comm., 2004), using age datums provided in Berggren et al. (1995). This biostratigraphy is fairly similar to that suggested on the ship (Bralower, Premoli Silva, Malone, et al., 2002) and renders average Paleocene–Eocene sedimentation rates of 1.5 m/m.y. in Hole 1211A and 3 m/m.y. in Hole 1209A (Shipboard Scientific Party,

F3. Lithologic logs, Sites 1209 and 1211, p. 15.

2002, p. 121). Values are typical for plateaus in open-ocean, deepwater settings (Kennett, 1982).

Sediments deposited during several critical episodes of Paleogene climate evolution (Fig. F1) were recovered in both Holes 1209A and 1211A (Fig. F2). These episodes include the Eocene/Oligocene transition, the EECO and the IETM, as well as a mid-Paleocene biotic event characterized by the first occurrence (FO) of the nannolith *Heliolithus kleinpellii* (58.4 Ma) and primitive discoasters, both of which are important, and often dominant, components of late Paleocene and younger nannoplankton assemblages. Sediment deposited during this biotic event also contains a low-diversity planktonic foraminiferal assemblage dominated by *Igorina tadjikastanensis* (Shipboard Scientific Party, 2002; Petrizzo, this volume).

An increase in carbonate content and a lack of color cycles highlights the Eocene/Oligocene transition. Although no obvious lithologic changes characterize the EECO, a thin claystone marks the IETM and a phillipsite-rich, carbonate-poor horizon containing abundant fish teeth and manganese-coated foraminifers marks the mid-Paleocene biotic event (Shipboard Scientific Party, 2002). Additionally, intervals of low sedimentation rate are found in middle to upper Eocene sediment between 33.7 and 45 Ma in both holes (M.R. Petrizzo, pers. comm., 2004).

For this study, we collected 134 sediment samples of 10 cm^3 from 137.56 to 251.38 mcd in Hole 1209A and 99 sediment samples of 10 cm^3 from 84.60 to 147.46 mcd in Hole 1211A (Fig. F3). Samples were initially taken onboard ship at a resolution of three per core. In order to examine a potential relationship between sediment cycles and dissolution, one sample was also taken from obvious light and dark layers. Additional samples were collected every 10 to 20 cm over suspected dissolution episodes. On average and from each hole, there are about four samples for every 1 m.y. of sediment deposition.

METHODS

Preparation

All samples were freeze-dried to remove water and divided into two portions. The first ~2-cm^3 portion was crushed and used to determine bulk carbonate content. The other ~5-cm^3 portion was weighed, wet-sieved at 38 µm, and used to determine coarse size fraction, benthic foraminiferal abundance, and foraminiferal fragmentation. All four of these parameters have been used in previous investigations to make inferences about carbonate dissolution (e.g., Le and Shackleton, 1992; LaMontagne et al., 1996). In studies of Quaternary foraminiferal assemblages, the >63-µm size fraction has generally been used for dissolution studies because it conveniently coincides with the sand size fraction (e.g., Broecker and Clark, 1999, 2001). However, 38 µm was chosen to delineate coarse fraction in this study because Paleocene foraminifers are commonly very small.

Carbonate Content

Approximately 100 mg of dried, crushed sample was analyzed for carbonate content according to the "Karbonate-Bomb" method (Mueller and Gastner, 1971). Sample aliquots were reacted with ~3 mL of 10% HCl to produce CO_2 gas in a closed vessel attached to a water-

filled cylinder marked with 0.1-mL graduations. Carbonate content was determined by comparing the volume of CO_2 gas generated to that produced from known masses of laboratory-grade $CaCO_3$. Each sample was analyzed twice to ensure analytical precision. These replicate analyses were consistently within 2 wt%, and reported carbonate contents are the average of both measurements. A sample of Paleogene siliceous limestone (JCU Sample MS14) with a known carbonate content of 72 wt% was also analyzed twice to evaluate accuracy and precision. The measured carbonate content of MS14 was 71 wt% ± 2 wt%.

Coarse Size Fraction and Microsplitting

After wet sieving, the coarse (>38 µm) component of the second sample portion was dried and weighed. This mass divided by bulk sample mass rendered the coarse (>38 µm) size fraction. Carbonate dissolution within the lysocline commonly leads to fragmentation of foraminifer tests, which decreases the coarse size fraction of bulk sediment (Berger et al., 1982; Broecker and Clark, 1999). However, we were unsure if and how this proxy would register dissolution in Paleogene sediment from Shatsky Rise because nannofossils are the dominant contributors (>90%) to the sediment (see "Visual Core Descriptions" in Bralower, Premoli Silva, Malone, et al., 2002). Changes in the relative abundances of nannofossils and foraminifers could certainly give variations in grain size unrelated to dissolution.

A microsplitter was then used to separate at least 300 foraminifers and fragments from the coarse fraction onto a marked slide. Care was taken to distribute material evenly over the microsplitter to avoid sampling bias. The numbers of fragments, benthic foraminifers, and planktonic foraminifers were recorded. Where the sample was highly fragmented and whole foraminifers rare, at least 50 counts of whole foraminifers were made.

Benthic Abundance

The relative abundance of benthic foraminifers (BENTH) is expressed as a ratio of benthic foraminifers to the sum of benthic and planktonic foraminifers. Benthic foraminifers are less susceptible to dissolution than planktonic foraminifers because the latter typically have porous chamber walls designed to maintain buoyancy in surface waters. Thus, the relative abundance of benthic foraminifers may serve as an index for carbonate dissolution at deepwater sites (Schlanger and Douglas, 1973; Thunell, 1976).

Foraminiferal Fragmentation

A foraminiferal fragment (F) is defined here and elsewhere (Berger et al., 1982) as a test portion less than two-thirds of its original size. The fragmentation index (FRAG) for each sample was calculated according to the following equation (Williams et al., 1985; Malmgren, 1987):

$$FRAG = (F/8)/[(F/8) + \text{whole planktonic foraminifers}].$$

The number of fragments is divided by 8 because, on average, one foraminifer breaks into this number of fragments and it is the proportion of fragmented foraminifers, rather than the number of fragments

themselves, that has a near-linear relationship with dissolution (Le and Shackleton, 1992). Benthic foraminifers are not included in the whole foraminifer count as their tests are more resistant to dissolution than planktonic foraminifers.

RESULTS

Carbonate content across all samples varies from 64 to 100 wt%. Values generally exceed 85 wt%, which is consistent with shipboard data (Bralower, Premoli Silva, Malone, et al., 2002) (Fig. F4; Tables T1, T2). Fluctuations between low and high carbonate content are more periodic at the shallower Site 1209, especially in middle to upper lower Eocene sediment. For Hole 1209A, the lowest carbonate contents were found in upper Paleocene sediment deposited at the base of planktonic foraminiferal Zone P4 (~59 Ma) and in middle Eocene sediment deposited at the base of Zone P14 (~40 Ma) (Fig. F4). For Hole 1211A, the lowest carbonate contents were found in middle Eocene sediment deposited at the base of Zone P12 (~43 Ma) (Fig. F4). The upper Paleocene sediment samples with low carbonate content contain abundant phillipsite, fish teeth, manganese-coated planktic foraminifers, and residual foraminiferal assemblages dominated by thick-walled species.

Grain size throughout both studied sequences is generally fine, with the coarse fraction varying from <1 to 40 wt%, but averaging 5 wt% (Fig. F5; Tables T1, T2). The typically small grain size is consistent with shipboard lithological descriptions, which classified the recovered Paleocene and Eocene sediment as nannofossil ooze (Bralower, Premoli Silva, Malone, et al., 2002). There are, however, several intervals particularly enriched in coarse-grained sediment. For both holes, the >38-μm fraction surpasses 31 wt% at the start of the Paleocene and 13 wt% at the start of the Eocene (Fig. F5).

Benthic foraminifer abundance varies considerably in the samples studied, ranging from <1% to 100% (Fig. F6; Tables T1, T2). In both holes, BENTH usually averages 20%, implying that planktonic species generally dominate Paleocene and Eocene foraminiferal assemblages. A wide range in BENTH occurs, however, because foraminiferal assemblages are comprised mostly of benthic species across several specific intervals, notably in planktonic foraminiferal Zone P4 (~59–58 and 56 Ma) and during the middle and late Eocene in Zones P12–P16 (specifically ~40 and 37–33.7 Ma) in both holes.

The fragmentation index varies from <1% to 100% but averages ~25% and is generally <10% for both sites (Fig. F7; Tables T1, T2). However, significant increases in FRAG were found in Zone P4 (~59–58 and 56 Ma) and during the middle and late Eocene (~37–33.7 Ma) for both holes. In Hole 1209A, FRAG also increases in the middle Eocene (~43 and 41 Ma), and in Hole 1211A, FRAG also increases in the late early Eocene (~51 Ma) and in the middle Eocene (~45 Ma).

RELIABILITY OF DISSOLUTION INDEXES

Of the dissolution indexes examined, FRAG and BENTH record greater-amplitude and higher-frequency variations than carbonate content or the proportion of coarse fraction (Figs. F4, F5, F6, F7). Presumably, FRAG and BENTH are more sensitive measures of carbonate
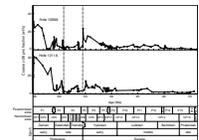
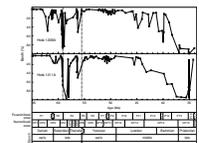F4. Carbonate content, Holes 1209A and 1211A, p. 16.
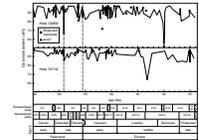
T1. Sample data, Hole 1209A, p. 21.
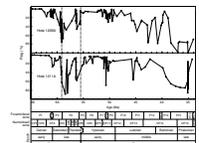
T2. Sample data, Hole 1211A, p. 23.

F5. Coarse fraction sediment, Holes 1209A and 1211A, p. 17.

F6. Dissolution of BENTH, Holes 1209A and 1211A, p. 18.

F7. Dissolution of FRAG, Holes 1209A and 1211A, p. 19.

dissolution because they can be high where carbonate content is high (e.g., LaMontagne et al., 1996), such as within the upper lysocline (Berger, 1967).

Plots between the various indexes, such as FRAG vs. each of carbonate content, size faction, and BENTH (Fig. F8), show some insights and complexities facing dissolution interpretations. Trends of FRAG and BENTH display a good correlation ($r^2 = 0.77$) across the sample set, and both probably provide good indicators of carbonate dissolution, at least for most samples in this study. However, planktonic and benthic counts are far less time consuming than fragmentation counts, so BENTH is a much easier measurement. A bivariate plot of FRAG and carbonate content shows a broad relationship of high carbonate content with low FRAG, but with weak correlation ($r^2 = 0.03$). At moderate to low carbonate content (<70 wt% for this study), FRAG may become problematic because significant numbers of fragments may have been dissolved and the residual assemblage can contain resistant tests. A plot of FRAG against coarse fraction shows that FRAG varies widely (0%–80%) when fine-grained material dominates bulk sediment (<10 wt% coarse) but is fairly constant when coarse-grained material comprises a significant fraction. As mentioned previously, the relative abundance of nannofossils complicates grain size interpretations in these sediments.

DISSOLUTION EPISODES

Paleocene and Eocene sediment sections at Sites 1209 and 1211 are relatively expanded and complete (Fig. F3). As suggested by the various proxy records for dissolution (Figs. F4, F5, F6, F7), this probably reflects a history where the two sites remained above the lysocline for good portions of the early Paleogene. Given estimated paleodepths of 2.0 km for Site 1209 and 2.5 km for Site 1211, this is consistent with a Pacific CCD deeper than 3.0 km during most of the Paleocene and Eocene (van Andel, 1975; Lyle, Wilson, Janacek, et al., 2002).

However, intervals of carbonate dissolution do punctuate the Paleocene and Eocene sediment sections on Shatsky Rise. When all four dissolution indexes are examined collectively, prominent dissolution occurred at both sites during the late Paleocene (lower Zone P4, ~59–58 Ma), and during the middle to late Eocene (Zones P11–P16, ~45–33.7 Ma). We discuss these two "dissolution episodes" below but note that intervals of enhanced carbonate dissolution also occurred during the late Paleocene (upper Zone P4, ~56 Ma), and the late early Eocene (Zone P7, ~51 Ma). The first of these other dissolution intervals immediately precedes the IETM. Interestingly, however, the IETM does not stand out in our records, as discussed below.

Considering the entire time interval examined, times of dissolution generally seem longer and more pronounced in Hole 1211A compared to Hole 1209A (Figs. F4, F5, F6, F7). This is consistent with the depth positions of the two sites.

Late Paleocene (~59–58 Ma)

Beginning close to the boundary between the P3 and P4 foraminiferal biozones (~59.1 Ma) and continuing for 1 to 2 m.y. afterwards, BENTH and FRAG are unusually high at both Site 1209 and Site 1211 (Figs. F6, F7). There are also noticeable drops in the carbonate content and coarse fraction of bulk sediment (Figs. F4, F5). At both sites
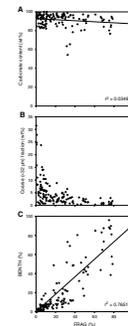
the dissolution episode closely coincides with the mid-Paleocene biotic event (Figs. F4, F5, F6, F7). Note that Petrizzo (this volume) dated the mid-Paleocene biotic event at ~58.4 Ma whereas the planktonic foraminiferal biostratigraphy used in this study (Berggren et al., 1995; M.R. Petrizzo, pers. comm., 2004) gives an age of ~59.1 Ma. The biotic event is characterized by high magnetic susceptibility, high abundances of phillipsite and manganese-coated foraminifers, and residual foraminiferal assemblages (Shipboard Scientific Party, 2002; Petrizzo, this volume). These sedimentological features further support carbonate dissolution and reduced sedimentation rates (Shipboard Scientific Party, 2002; Petrizzo, this volume). Thus, all information suggests that the lysocline shoaled significantly during this time.

Importantly, carbonate dissolution as measured in our study extends several meters beyond the biotic event as defined by obvious lithological change. For example, in Hole 1209A, the zone of high magnetic susceptibility and phillipsite spans from ~212.30 to 211.85 mbsf, whereas BENTH and FRAG generally exceed 25% from 215.80 to 210.90 mbsf. Thus, it appears that the biotic event marks a brief extreme within the context of a longer, 1- to 2-m.y. interval of unusual conditions. The relatively long time supports the view of Petrizzo (this volume) that the biotic event and its coeval carbonate dissolution were somehow linked to a change in ocean circulation, rather than a massive input of carbon such as occurred at the IETM. We note that an unusual black shale facies closely corresponds to the start of the P4 foraminiferal biozone in sections deposited off the east coast of New Zealand and that this also has been attributed to a change in Pacific circulation (Hollis et al., 2005).

Middle to Late Eocene (~45–33.7 Ma)

All indexes for dissolution also suggest a relative shoaling of the lysocline in the late Eocene beginning at ~45 Ma and becoming particularly prominent between 37 and 33.7 Ma. Support for such dissolution on Shatsky Rise comes from sedimentation rates, which drop significantly across this horizon at Sites 1209, 1210, 1211, and 1212 (Bralower, Premoli Silva, Malone, et al., 2002).

Site 711 on Madingley Rise in the Central Indian Ocean also contains a condensed interval of low carbonate accumulation during the late Eocene (Peterson et al., 1992). This may hint at a correlative shoaling of the lysocline in this basin. Furthermore, existing CCD records for the Pacific and Indian Oceans (van Andel, 1975; Lyle, Wilson, Janacek, et al., 2002) indicate an anomalously shallow CCD of ~3.2 km for the late Eocene. Although the exact shapes of the CCD and lysocline through the early Paleogene remain poorly constrained, both probably shoaled between 45 and 33.7 Ma, perhaps to minimum depths between 37 and 33.7 Ma.

The magnitude and longevity of this middle to late Eocene dissolution interval suggests a change in the ocean carbonate budget, which may ultimately relate to alkalinity and Ca inputs. Interestingly, this time interval was characterized by significant cooling and the first ephemeral ice sheets on Antarctica (Zachos et al., 1994, 2001). One explanation is that this represents a time of relatively high sea level but reduced weathering, so that the limited inputs were predominantly stored on the shelves.

Initial Eocene Thermal Maximum (~55.5 Ma)

At Sites 1209 and 1211, the IETM (~55.5 Ma in this study) is marked by an ~12-cm layer of clayey nannofossil ooze with a sharp basal contact, a 1-mm clay layer, and a gradational upper contact (Shipboard Scientific Party, 2002). Additionally, nannofossil preservation decreases toward the base of this unit (Shipboard Scientific Party, 2002). The lysocline probably shoaled significantly and rapidly during the IETM on Shatsky Rise (Colosimo et al., this volume) and in all regions of the ocean in response to massive carbon addition (Dickens et al., 1997; Dickens 2000).

Our records do not express this lysocline shoaling very well, probably for two related reasons. First, the IETM is poorly represented in Holes 1209A and 1211A (e.g., core recovery and splitting appear to have disturbed the clay seam in Hole 1209A) (Shipboard Scientific Party, 2002). Second, we did not examine the base of the interval with appropriate sample resolution. Interestingly, though, BENTH and FRAG both drop significantly within 10–20 cm above the start of the IETM (Figs. F6, F7). This interval also has a corresponding influx of well-preserved planktonic foraminifers, which increase the >38-μm fraction (Fig. F5). Together, these observations may indicate a deepening of the lysocline immediately following the initial lyscoline shoaling and carbon addition. Carbon cycle models that include a weathering feedback, where increased CO_2 in the atmosphere accelerates continental weathering, predict such a change in the lysocline (Dickens et al., 1997).

SUMMARY AND CONCLUSIONS

Indexes for carbonate dissolution were examined in lower Paleogene sediment (65–33.7 Ma) recovered from two boreholes (1209A and 1211A) on Shatsky Rise. The two best measures for carbonate dissolution are probably FRAG and BENTH, which indicate the relative abundance of foraminifer test fragmentation and benthic foraminifers, respectively. These proxies display good covariance across the sample set and similar downhole patterns in Holes 1209A and 1211A.

For Holes 1209A and 1211A, all indexes suggest two significant early Paleogene dissolution episodes. The first of these occurred in the early late Paleocene at ~59–58 Ma (lower part of planktonic foraminifer Zone P4) and coincides with a recently identified biotic event. We suspect that the biotic event and accompanying seafloor carbonate dissolution relate to a change in deep ocean circulation. The second dissolution episode begins in the middle Eocene at ~45 Ma (Zone P11) but reaches a maxima during the late Eocene at ~37–33.7 Ma (Zones P15–P16). This is probably the most prominent interval of carbonate dissolution recorded in Paleogene sediments from Shatsky Rise and may represent a time of shallow lysoclines and CCDs throughout the oceans. Other intervals of enhanced carbonate dissolution occurred in the late Paleocene at ~56 Ma (upper Zone P4) and in the late early Eocene at ~51 Ma (Zone P7). The IETM interval was not really investigated in this study, but the lysocline may have first shoaled then deepened.

ACKNOWLEDGMENTS

REFERENCES

Berger, W.H., 1967. Foraminiferal ooze: solution at depths. *Science,* 156:383–385.

Berger, W.H., 1971. Sedimentation of planktonic foraminifera. *Mar. Geol.,* 11:325–358.

Berger, W.H., 1974. Plate stratigraphy and the fluctuating carbonate line. *Spec. Publ. Int. Assoc. Sedimentol.,* 1:11–48.

Berger, W.H., 1992. Pacific carbonate cycles revisited: arguments for and against productivity control. *In* Ishizaki, K., and Saito, T. (Eds.), *Centenary of Japanese Micropaleontology:* Tokyo (Terra Sci.), 15–25.

Berger, W.H., Bonneau, M.-C., and Parker, F.L., 1982. Foraminifera on the deep-sea floor: lysocline and dissolution rate. *Oceanol. Acta,* 5(2):249–258.

Berggren, F.C., Kent, D.V., Swisher, C.C., III, and Aubry, M.-P., 1995. A revised Cenozoic geochronology and chronostratigraphy. *In* Berggren, W.A., Kent, D.V., Aubry, M.-P., and Hardenbol, J. (Eds.), *Geochronology, Time Scales and Global Stratigraphic Correlation.* Spec Publ.—SEPM (Soc. Sediment. Geol.), 54:129–212.

Bralower, T.J., Premoli Silva, I., Malone, M.J., et al., 2002. *Proc. ODP, Init. Repts.,* 198 [CD-ROM]. Available from: Ocean Drilling Program, Texas A&M University, College Station TX 77845-9547, USA.

Bramlette, M.N., 1961. Pelagic sediments. *In* Sears, M. (Ed.), *Oceanography.* Am. Assoc. Adv. Sci. Publ., 67:345–366.

Broecker, W.S., and Clark, E., 1999. $CaCO_3$ size distribution: a paleocarbonate ion proxy? *Paleoceanography,* 14(5):596–604.

Broecker, W.S., and Clark, E., 2001. Reevaluation of the $CaCO_3$ size index paleocarbonate ion proxy. *Paleoceanography,* 16(6):669–671.

Dickens, G.R., 2000. Methane oxidation during the late Palaeocene Thermal Maximum. *Bull. Soc. Geol. Fr.,* 171:37–49.

Dickens, G.R., Castillo, M.M., and Walker, J.C.G., 1997. A blast of gas in the latest Paleocene: simulating first-order effects of massive dissociation of oceanic methane hydrate. *Geology,* 25(3):259–262.

Farrell, J.W., and Prell, W.L., 1989. Climatic change and $CaCO_3$ preservation: An 800,000 year bathymetric reconstruction from the central equatorial Pacific Ocean. *Paleoceanography,* 4(4):447–466.

Hollis, C.J., Dickens, G.R., Field, B.C., Jones, C.M., and Strong, C.P., 2005. The Paleocene-Eocene transition at Mead Stream, New Zealand: a southern Pacific record of early Cenozoic global change. *Palaeogeogr., Palaeoclimatol., Palaeoecol.,* 215:313–343.

Ito, G., and Clift, P.D., 1998. Subsidence and growth of Pacific Cretaceous plateaus. *Earth Planet. Sci. Lett.,* 161(1–4):85–100.

Kennett, J.P., 1982. *Marine Geology:* Englewood Cliffs, NJ (Prentice-Hall).

Kennett, J.P., and Stott, L.D., 1991. Abrupt deep-sea warming, paleoceanographic changes and benthic extinctions at the end of the Palaeocene. *Nature,* 353:225–229.

Kobashi, T., Grossman, E.L., Dockery, D.T., III, and Ivany, L.C., 2004. Water mass stability reconstructions from greenhouse (Eocene) to icehouse (Oligocene) for the northern Gulf Coast continental shelf (USA). *Paleoceanography,* 19(PA1022):10.1029/2003PA000934.

Krasheninnikov, V.A., 1981. Paleogene planktonic foraminifers from Deep Sea Drilling Project Leg 62 sites and adjacent areas of the Northwest Pacific. *In* Thiede, J., and Vallier, T.L. (Eds.), *Init. Repts. DSDP,* 62: Washington (U.S. Govt. Printing Office), 365–376.

LaMontagne, R.W., Murray, R.W., Wei, K.-Y., Leinen, M., and Wang, C.-H., 1996. Decoupling of carbonate preservation, carbonate concentration, and biogenic accumulation: a 400-kyr record from the central equatorial Pacific Ocean. *Paleoceanography,* 11(5):553–562.

Larson, R.L., Moberly, R., et al., 1975. *Init. Repts. DSDP,* 32: Washington (U.S. Govt. Printing Office).

Larson, R.L., Steiner, M.B., Erba, E., and Lancelot, Y., 1992. Paleolatitudes and tectonic reconstructions of the oldest portion of the Pacific plate: a comparative study. *In* Larson, R.L., Lancelot, Y., et al., *Proc. ODP, Sci. Results,* 129: College Station, TX (Ocean Drilling Program), 615–631.

Le, J., and Shackleton, N.J., 1992. Carbonate dissolution fluctuations in the western equatorial Pacific during the late Quaternary. *Paleoceanography,* 7(1):21–42.

Lyle, M., Wilson, P.A., Janecek, T.R., et al., 2002. *Proc. ODP, Init. Repts.,* 199 [CD-ROM]. Available from: Ocean Drilling Program, Texas A&M University, College Station TX 77845-9547, USA.

Malmgren, B.A., 1987. Differential dissolution of Upper Cretaceous planktonic foraminifera from a temperate region of the South Atlantic Ocean. *Mar. Micropaleontol.,* 11(4):251–271.

Mueller, G., and Gastner, M., 1971. The "Karbonate-Bombe," a simple device for the determination of the carbonate content in sediments, soils, and other materials. *Neues Jahrb. Mineral.,* 10:466–469.

Murray, J., and Renard, A.F., 1891. Deep-sea deposits based on the specimens collected during the voyage of *H.M.S. Challenger* in the years 1872 to 1876. *Rep. Voy. Challenger:* London (Longmans).

Peterson, L.C., Murray, D.W., Ehrmann, W.U., and Hempel, P., 1992. Cenozoic carbonate accumulation and compensation depth changes in the Indian Ocean. *In* Duncan, R.A., Rea, D.K., Kidd, R.B., von Rad, U., and Weissel, J.K. (Eds.), *Synthesis of Results from Scientific Drilling in the Indian Ocean.* Geophys. Monogr., 70:311–333.

Peterson, M.N.A., 1966. Calcite—rates of dissolution in a vertical profile in the central Pacific. *Science,* 154:1542–1544.

Sager, W.W., Kim, J., Klaus, A., Nakanishi, M., and Khankishieva, L.M., 1999. Bathymetry of Shatsky Rise, northwest Pacific Ocean: implications for ocean plateau development at a triple junction. *J. Geophys. Res., [Solid Earth],* 104(4):7557–7576.

Schlanger, S.O., and Douglas, R.G., 1973. Porosity and textural changes related to the ooze-chalk-limestone transition. *Eur. Geophys. Soc. Meet. Abstr.,* 1:92.

Schmitz, B., Speijer, R.P., and Aubry, M.-P., 1996. Latest Paleocene benthic extinction event on the southern Tethyan shelf (Egypt): foraminiferal stable isotopic (δ^{13}C, δ^{18}O) records. *Geology,* 24:347–350.

Shipboard Scientific Party, 2002. Leg 198 summary. *In* Bralower, T.J., Premoli Silva, I., Malone, M.J., et al., *Proc. ODP, Init. Repts.,* 198: College Station TX (Ocean Drilling Program), 1–148.

Sliter, W.V., and Brown, G.R., 1993. Shatsky Rise: seismic stratigraphy and sedimentary record of Pacific paleoceanography since the Early Cretaceous. *In* Natland, J.H., Storms, M.A., et al., *Proc. ODP, Sci. Results,* 132: College Station, TX (Ocean Drilling Program), 3–13.

Thomas, E., and Shackleton, N., 1996. The Palaeocene–Eocene benthic foraminiferal extinction and stable isotope anomalies. *In* Knox, R.W.O'B., Corfield, R.M., and Dunay, R.E. (Eds.), *Correlation of the Early Paleogene in Northwest Europe.* Geol. Soc. Spec. Publ., 101:401–441.

Thunell, R.C., 1976. Optimum indices of calcium carbonate dissolution in deep-sea sediments. *Geology,* 4(9):525–528.

van Andel, T.H., 1975. Mesozoic/Cenozoic calcite compensation depth and the global distribution of calcareous sediments. *Earth Planet. Sci. Lett.,* 26:187–194.

Williams, D.F., Healy-Williams, N., and Leschak, P., 1985. Dissolution and water-mass patterns in the Southeast Indian Ocean. Part I. Evidence from Recent to late Holocene foraminiferal assemblages. *Geol. Soc. Am. Bull.,* 96(2):176–189.

Zachos, J., Pagani, M., Sloan, L., Thomas, E., and Billups, K., 2001. Trends, rhythms, and aberrations in global climate 65 Ma to present. *Science,* 292(5517):686–693.

Zachos, J.C., Stott, L.D., and Lohmann, K.C., 1994. Evolution of early Cenozoic marine temperatures. *Paleoceanography,* 9(2):353–387.

Figure F1. Paleocene and Eocene geochronology (following Berggren et al., 1995) with global carbon and oxygen isotope curves constructed using benthic foraminifer isotope data (adapted from Zachos et al., 2001). Three key intervals of changing climate and carbon cycling are noted: PCIM = Paleocene Carbon Isotope Maximum, IETM = Initial Eocene Thermal Maximum, EECO = Early Eocene Climatic Optimum.
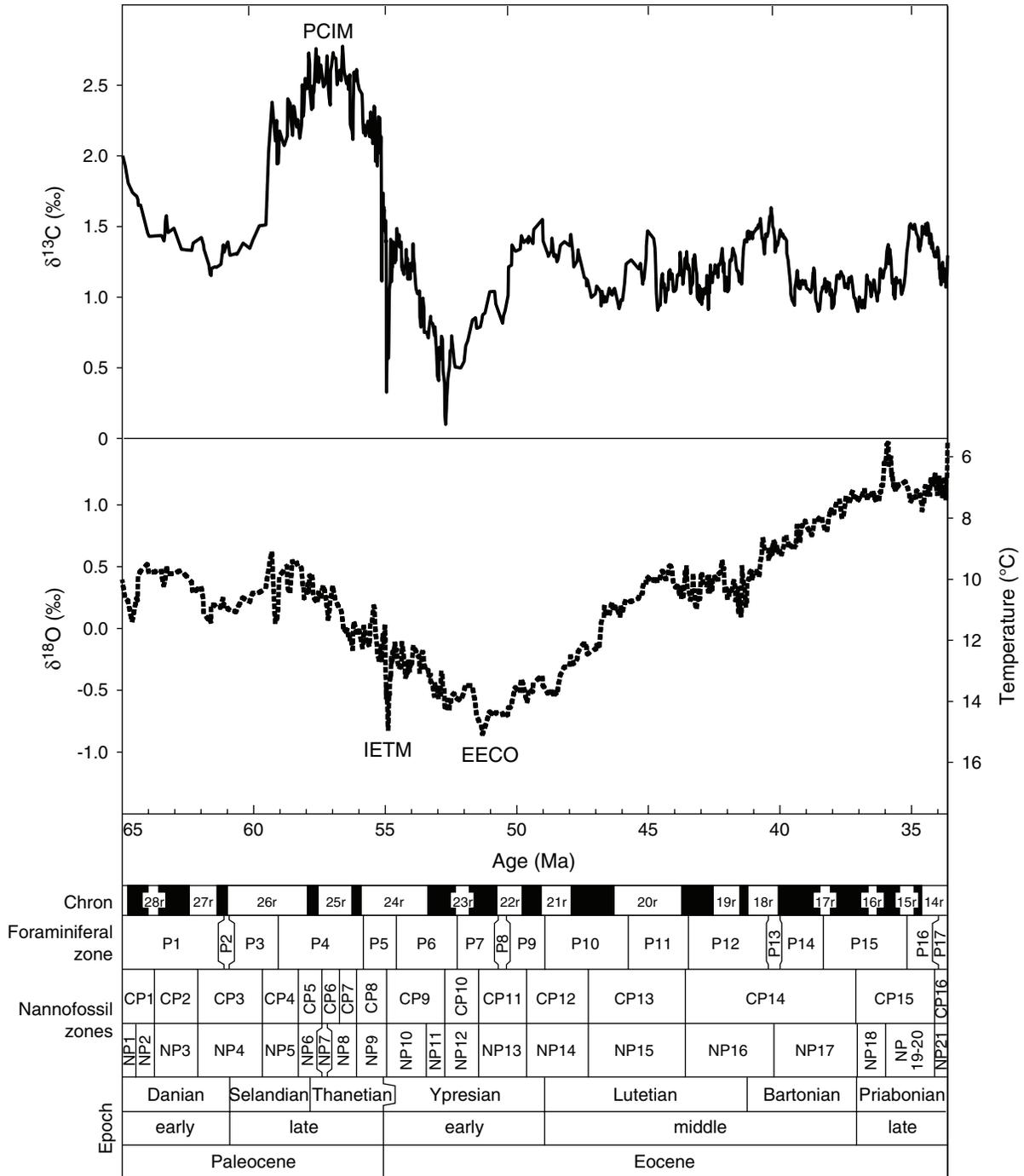
Figure F2. Location of Sites 1209 and 1211 on the Southern High, Shatsky Rise (adapted from Shipboard Scientific Party, 2002).
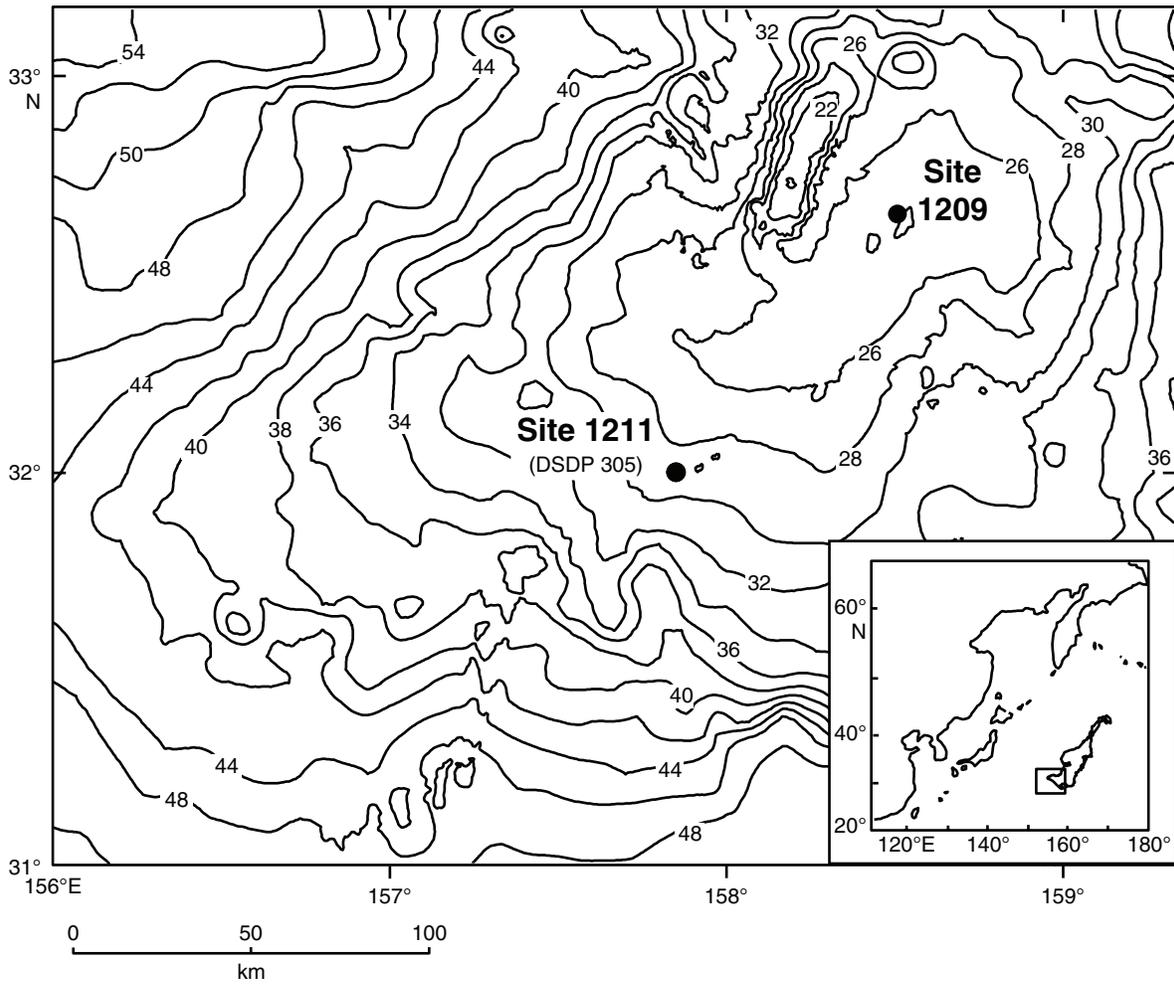
Figure F3. Lithologic logs for Sites 1209 and 1211 with planktonic foraminifer (M.R. Petrizzo, pers. comm., 2004) and nannofossil datums (T.S. Bralower, pers. comm., 2004).
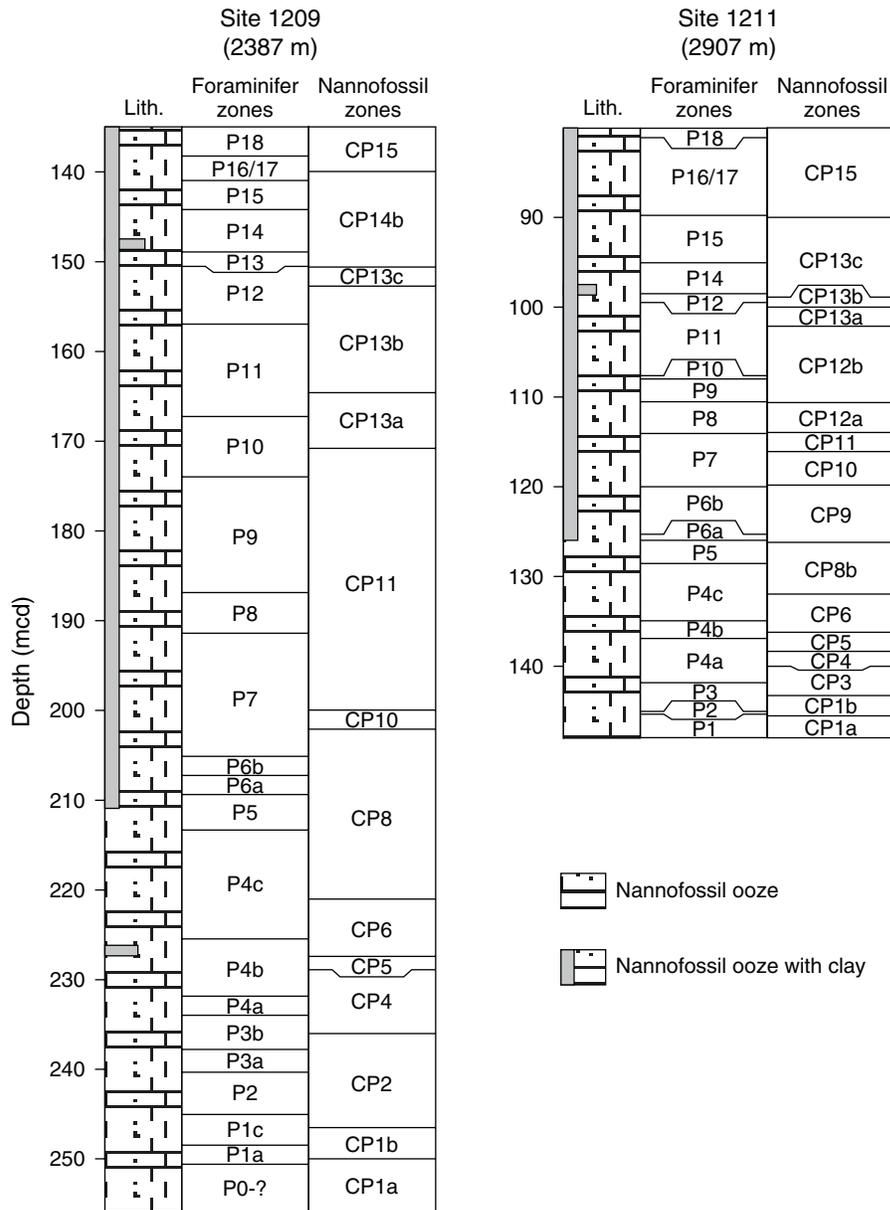
Figure F4. Carbonate content in Paleocene and Eocene sediment in Holes 1209A and 1211A.
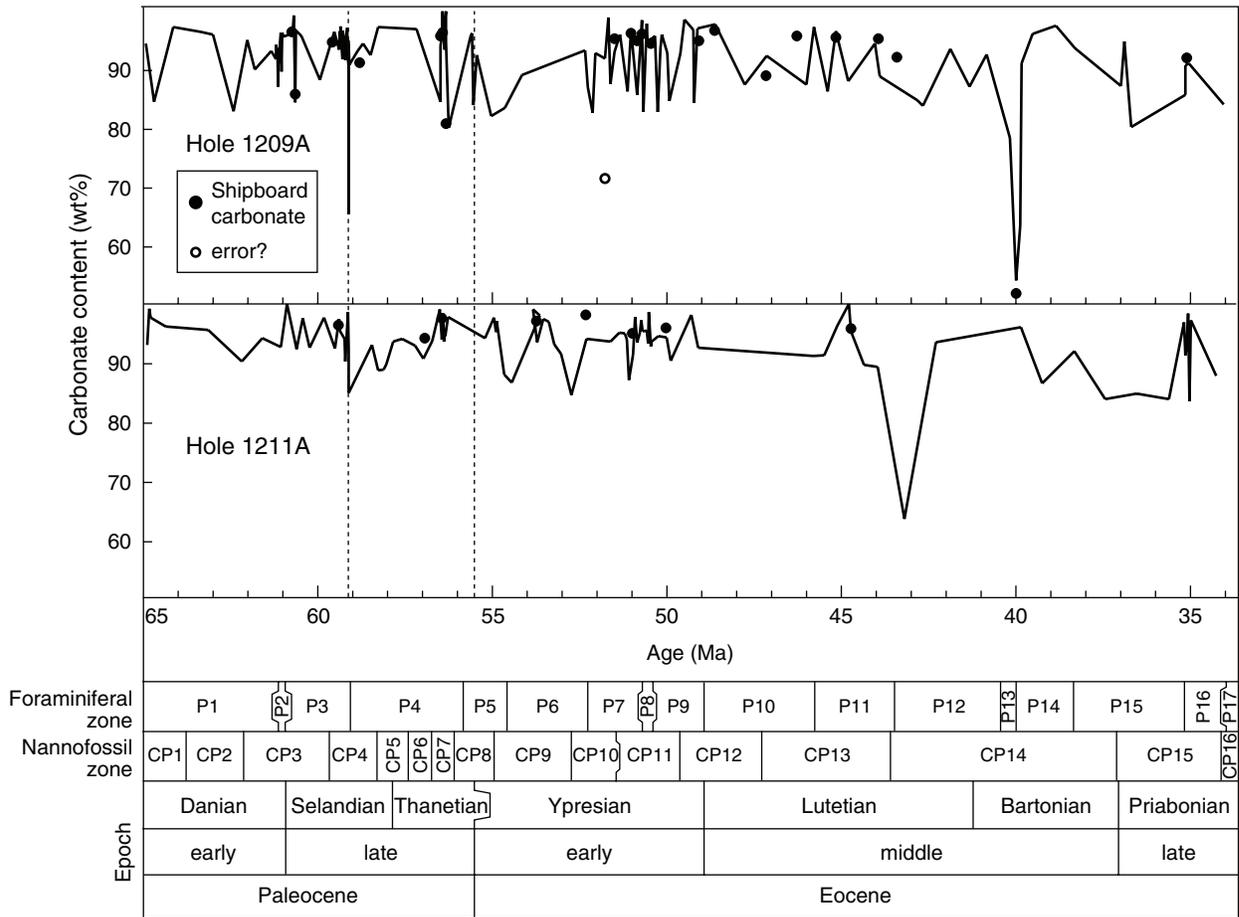
Figure F5. Coarse fraction of sediment in Paleocene and Eocene sediment in Holes 1209A and 1211A.

Figure F6. The dissolution proxy BENTH in Paleocene and Eocene sediment in Holes 1209A and 1211A.

Figure F7. The dissolution proxy FRAG in Paleocene and Eocene sediment in Holes 1209A and 1211A.

Figure F8. Bivariant plots of potential dissolution indexes. **A.** FRAG vs. Carbonate content. **B.** FRAG vs. Coarse fraction. **C.** FRAG vs. BENTH.

Table T1. Sample, depths, age and dissolution indexes, Hole 1209A. (Continued on next page.)

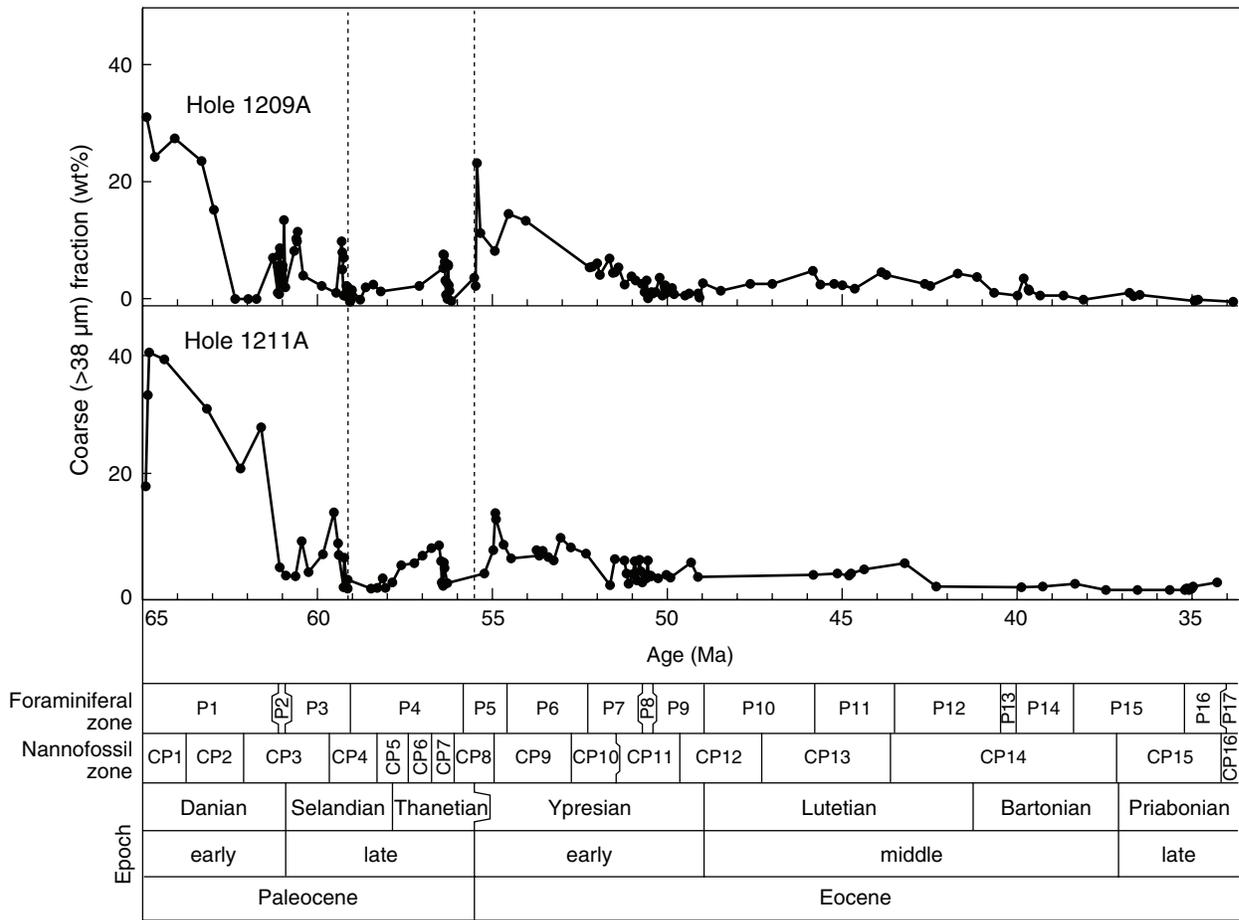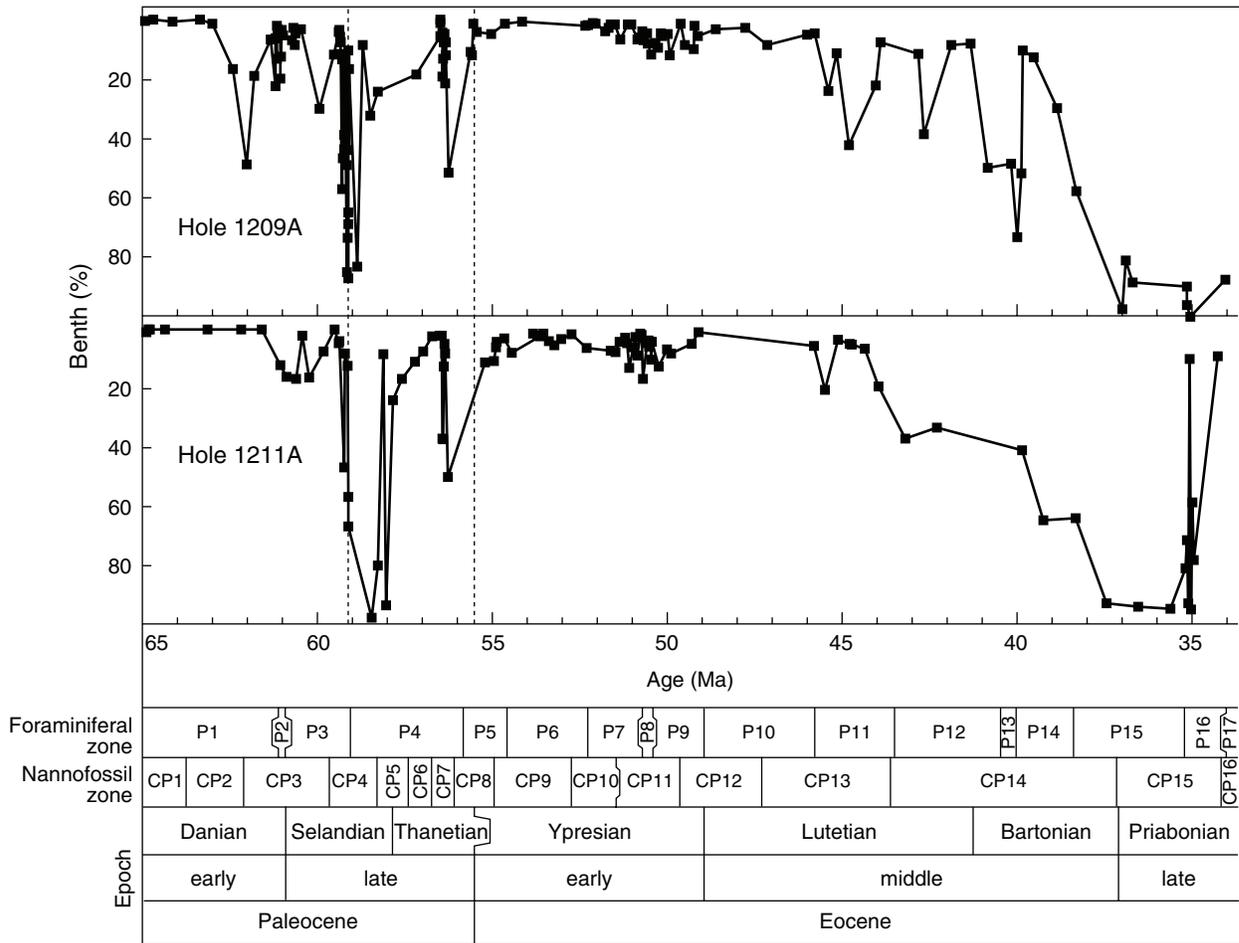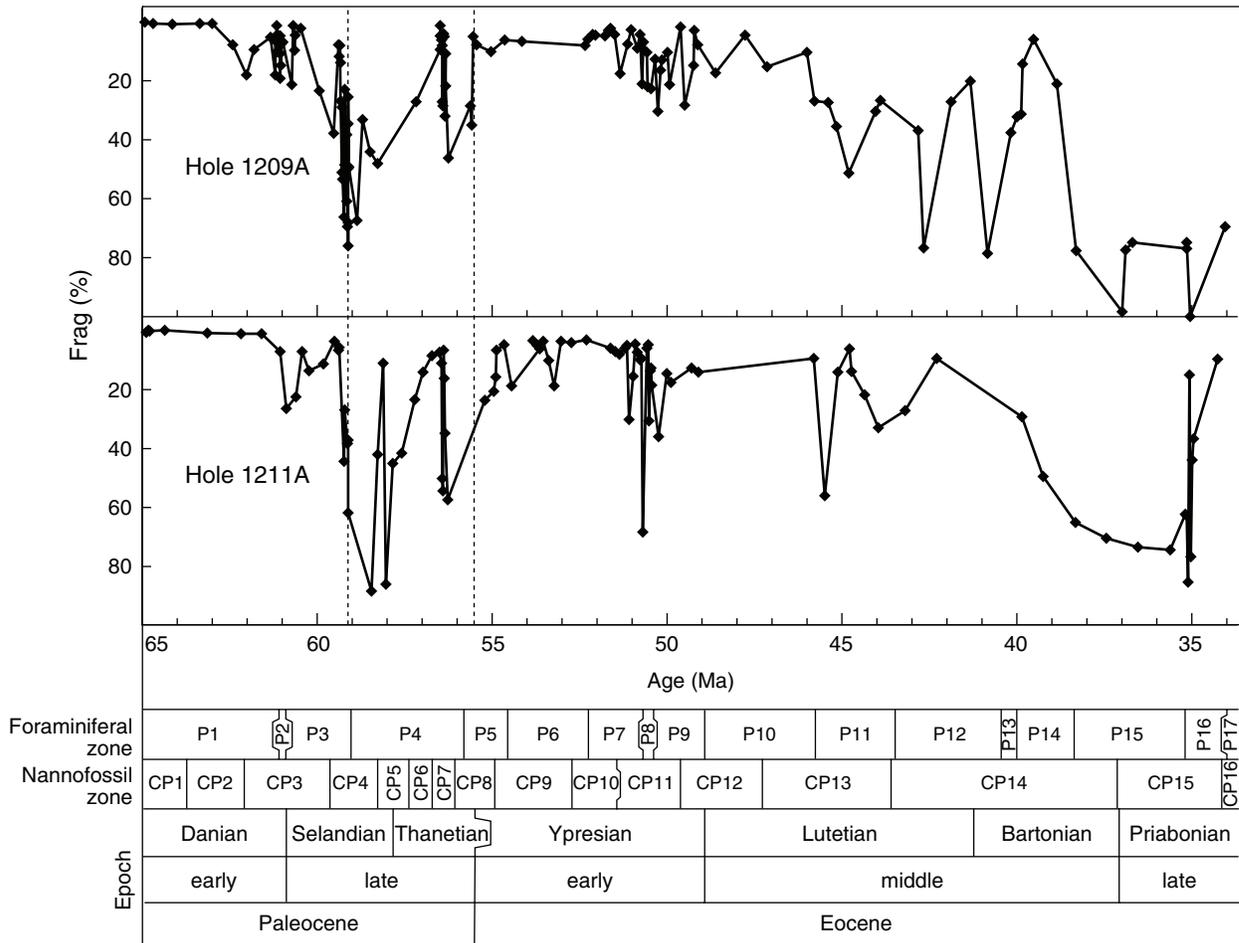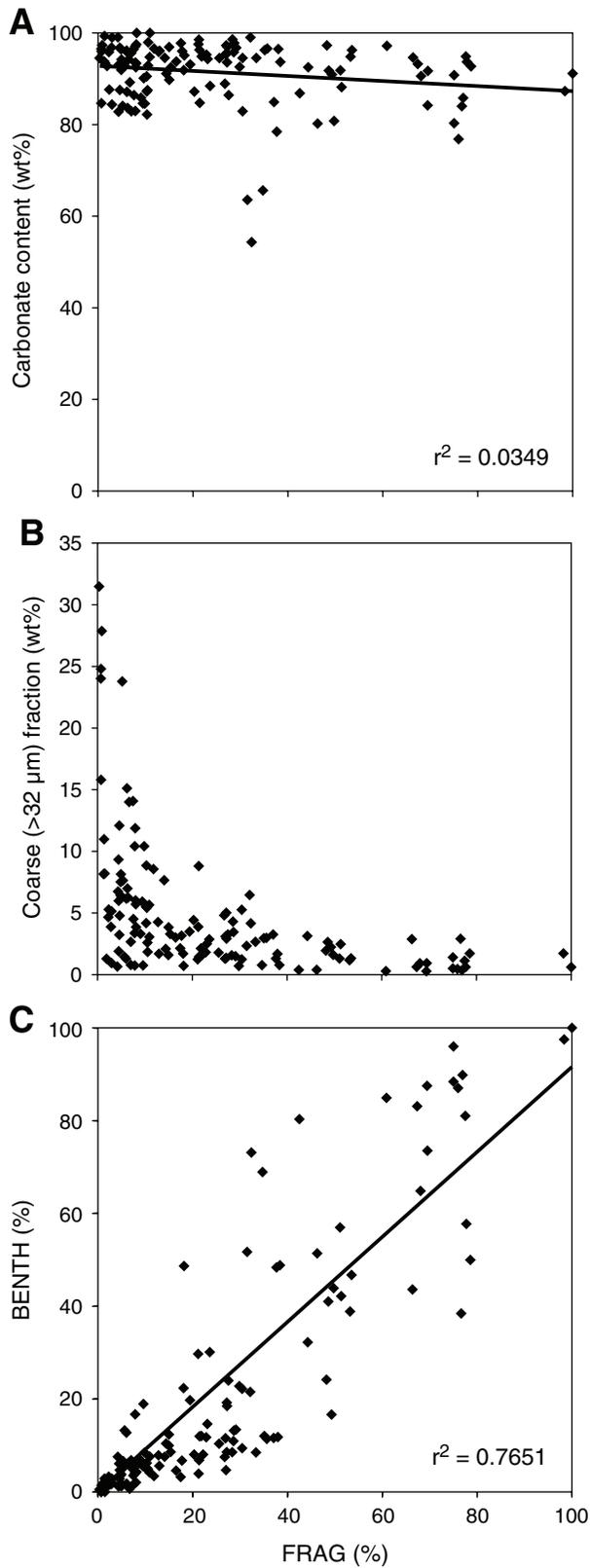| Core, section, interval (cm)	Depth (mbsf)	Depth (mcd)	Age (Ma)	Fragment (%)	Benthic (%)	Coarse fraction (>38µm) (wt%)	Carbonate content (wt%)
198-1209A-							
14H-5, 67–69	128.87	139.06	34.04	69.4	87.5	0.3	84.2
14H-6, 67–69	130.37	140.56	35.04	100.0	100.0	0.6	91.2
14H-6, 82–84	130.52	140.71	35.13	75.0	96.0	0.5	90.8
15H-1, 67–69	132.37	140.68	35.13	76.9	89.8	0.4	85.8
15H-2, 67–69	133.87	142.18	36.69	75.0	88.4	1.4	80.3
15H-2, 85–87	134.05	142.36	36.88	77.5	81.0	1.1	94.9
15H-2, 95–97	134.15	142.46	36.99	98.4	97.5	1.7	87.3
15H-3, 67–69	135.37	143.68	38.30	77.7	57.8	0.6	93.7
15H-4, 69–71	136.89	145.20	38.86	21.1	29.7	1.2	97.5
15H-5, 122–124	138.92	147.23	39.52	6.0	12.8	1.3	96.1
15H-6, 72–74	139.92	148.23	39.84	14.4	10.4	2.1	91.1
15H-6, 80–82	140.00	148.31	39.87	31.5	51.7	2.3	63.6
15H-7, 20–22	140.40	148.71	40.00	32.4	73.1	4.2	54.3
15H-CC, 2–4	140.98	149.29	40.17	37.7	48.4	1.3	78.4
16H-1, 45–47	141.65	151.22	40.83	78.6	50.0	1.7	92.7
16H-2, 67–69	142.66	152.23	41.33	20.3	8.1	4.4	87.2
16H-3, 27–29	143.76	153.33	41.87	27.2	8.6	5.0	93.6
16H-4, 36–38	145.35	154.92	42.66	76.6	38.5	2.9	84.0
16H-4, 67–69	145.66	155.23	42.81	37.1	11.6	3.3	84.9
16H-6, 67–69	148.66	158.23	43.90	26.7	7.5	4.8	88.9
16H-7, 30–32	149.29	158.86	44.03	30.4	22.2	5.3	94.5
17H-1, 55–57	151.25	162.49	44.80	51.3	42.2	2.5	88.2
17H-2, 67–69	152.87	164.11	45.14	35.6	11.4	3.0	96.6
17H-3, 32–34	154.02	165.26	45.39	27.5	24.0	3.3	86.4
17H-4, 67–69	155.87	167.11	45.78	27.0	4.7	3.1	97.3
17H-4, 117–119	156.37	167.61	45.99	10.4	5.1	5.4	87.5
17H-6, 67–69	158.87	170.11	47.13	15.3	8.6	3.3	92.5
17H-7, 55–57	160.25	171.49	47.76	4.6	2.8	3.2	87.6
18H-2, 67–69	162.37	173.35	48.61	17.5	3.2	2.1	97.8
18H-3, 107–109	164.27	175.25	49.12	7.8	5.5	3.4	97.0
18H-4, 47–49	165.17	176.15	49.22	2.9	2.1	0.9	84.4
18H-4, 69–71	165.39	176.37	49.24	15.0	10.0	1.6	96.9
18H-6, 73–75	167.72	178.70	49.50	28.3	8.5	1.6	98.6
18H-7, 20–22	168.69	179.67	49.61	1.9	1.4	1.3	92.8
19H-1, 30–32	170.00	182.53	49.93	21.4	12.0	1.5	84.7
19H-1, 85–87	170.55	183.08	49.99	10.5	4.8	2.6	92.9
19H-2, 70–72	171.90	184.43	50.14	13.0	5.6	1.7	96.1
19H-2, 105–107	172.25	184.78	50.18	16.5	4.6	3.0	93.8
19H-3, 21–23	172.91	185.44	50.25	30.4	9.4	1.2	82.9
19H-3, 92–94	173.62	186.15	50.33	12.8	7.9	4.3	95.9
19H-4, 69–71	174.89	187.42	50.46	22.8	11.8	1.8	95.3
19H-5, 22.5–24.5	175.93	188.46	50.54	22.2	8.1	1.6	95.2
19H-5, 62.5–64.5	176.32	188.86	50.58	10.6	4.7	1.8	97.9
19H-6, 31–33	177.51	190.04	50.68	7.0	6.8	0.8	82.9
19H-6, 73–75	177.93	190.46	50.71	21.2	3.9	3.9	98.5
19H-7, 42–44	178.62	191.15	50.77	4.5	6.1	1.9	93.1
20H-1, 63–65	179.83	191.98	50.85	9.1	6.8	3.3	85.9
20H-2, 67–69	181.37	193.52	51.02	2.8	1.7	3.9	96.8
20H-3, 25–27	182.45	194.60	51.13	7.6	1.7	4.5	86.4
20H-4, 66–68	184.36	196.51	51.34	17.7	6.7	3.2	96.0
20H-5, 72–74	185.92	198.07	51.50	4.5	1.5	6.0	93.2
20H-6, 28–30	186.98	199.13	51.62	2.3	1.5	5.3	87.6
20H-6, 72–74	187.42	199.57	51.66	3.0	2.8	5.1	99.0
20H-7, 15–17	188.35	200.50	51.76	4.9	3.8	7.5	91.9
21H-1, 120–122	189.90	203.11	52.04	4.7	1.4	4.8	92.9
21H-2, 40–42	190.60	203.81	52.12	4.3	1.2	6.7	82.8
21H-3, 15–17	191.85	205.06	52.25	6.1	1.8	6.2	87.1
21H-3, 61–63	192.31	205.52	52.33	8.0	2.0	6.0	93.4
21H-4, 67–69	193.87	207.08	54.14	6.7	0.7	14.0	89.2
21H-5, 67–69	195.37	208.58	54.63	6.2	1.5	15.1	83.6
21H-6, 30–32	196.50	209.71	55.03	10.3	4.9	8.9	82.2
21H-6, 140–142	197.60	210.81	55.43	7.9	4.1	11.9	92.5
21H-7, 19–21	197.89	211.10	55.54	5.2	1.5	23.8	84.1
21H-7, 29–31	197.99	211.20	55.57	35.1	12.0	3.0	96.3
21H-7, 40–42	198.10	211.31	55.61	28.6	11.0	4.3	95.8
22H-1, 66–68	198.86	213.06	56.25	46.3	51.4	0.4	80.2

Table T1 (continued).

Core, section, interval (cm)	Depth		Age (Ma)	Fragment (%)	Benthic (%)	Coarse fraction (>38µm) (wt%)	Carbonate content (wt%)
	(mbsf)	(mcd)					
22H-2, 22.5–24.5	199.93	214.13	56.32	21.8	12.0	2.1	94.9
22H-2, 68–70	200.38	214.58	56.32	10.9	7.6	3.1	100.0
22H-3, 42–44	201.62	215.82	56.34	32.1	21.5	6.5	99.0
22H-3, 132–134	202.52	216.72	56.36	5.1	4.9	6.2	93.5
22H-4, 70–71	203.40	217.60	56.38	4.2	7.6	0.7	99.0
22H-5, 37.5–39.5	204.57	218.78	56.40	28.7	13.2	3.5	97.8
22H-6, 141.5–143.5	205.62	219.82	56.41	27.2	19.2	1.4	95.6
22H-7, 69–71	206.39	220.59	56.43	8.1	4.3	3.9	100.0
23H-1, 50–52	207.20	221.40	56.44	6.3	6.0	7.0	95.6
23H-1, 20–22	207.90	223.55	56.48	4.9	1.3	8.1	94.2
23H-1, 38–40	208.08	223.73	56.48	1.5	0.0	8.2	93.4
23H-2, 80–82	208.50	224.15	56.49	9.5	5.6	5.9	84.6
23H-3, 66–68	209.86	225.51	57.17	27.2	18.5	2.9	97.0
23H-3, 21–23	210.91	226.56	58.26	48.2	24.2	2.0	97.3
23H-3, 42–44	211.12	226.77	58.48	44.3	32.3	3.1	92.5
23H-3, 62–64	211.32	226.97	58.69	33.3	8.5	2.7	94.5
23H-3, 77.5–79.5	211.48	227.13	58.85	67.3	83.1	0.6	93.2
23H-3, 100–102	211.70	227.35	59.08	49.3	16.7	2.2	90.9
23H-3, 110–112	211.80	227.45	59.10	25.6	10.4	1.8	94.5
23H-3, 120–122	211.90	227.55	59.11	49.7	43.9	1.6	80.8
23H-3, 130–132	212.00	227.65	59.11	34.7	68.9	0.8	65.6
23H-3, 140–142	212.10	227.75	59.12	76.0	87.0	0.5	76.8
23H-4, 147.5–149.5	212.18	227.83	59.12	68.0	64.9	0.9	90.6
23H-4, 11–13	212.31	227.96	59.13	69.5	73.5	0.9	91.7
23H-4, 48–50	212.68	228.33	59.14	38.4	48.9	0.8	93.7
23H-5, 67–69	212.87	228.52	59.15	60.9	84.9	0.3	97.2
23H-5, 21–23	213.91	229.56	59.20	23.1	14.6	2.5	94.3
23H-5, 41.5–43.5	214.12	229.77	59.21	48.6	41.0	2.7	91.8
23H-5, 80–82	214.50	230.15	59.23	53.2	38.9	1.2	94.8
23H-6, 102.5–104.5	214.73	230.38	59.24	66.4	43.6	2.9	94.6
23H-6, 20–22	215.40	231.05	59.27	53.5	46.7	1.3	96.3
23H-6, 60–62	215.80	231.45	59.29	29.1	13.4	1.5	96.8
23H-6, 67–69	215.87	231.52	59.29	51.1	57.0	1.3	91.8
23H-7, 140–142	216.60	232.25	59.32	26.9	11.6	1.3	95.4
24H-1, 58–60	217.28	232.93	59.35	8.1	5.7	5.7	97.5
24H-1, 10–12	217.30	232.33	59.33	14.1	7.6	7.7	94.6
24H-1, 85–87	218.05	233.08	59.36	11.8	3.4	8.6	96.6
24H-2, 135–137	218.55	233.58	59.38	7.9	4.1	10.4	93.5
24H-3, 65–67	219.35	234.38	59.53	38.0	11.8	1.7	96.5
24H-4, 47.5–49.5	220.68	235.71	59.94	23.6	30.1	2.9	88.4
24H-5, 66–68	222.36	237.39	60.47	2.3	3.3	4.7	95.8
24H-5, 5–7	223.25	238.28	60.63	4.6	4.7	12.1	96.8
24H-5, 11–13	223.31	238.34	60.64	9.9	8.5	10.4	84.6
24H-6, 30–32	223.50	238.53	60.67	1.4	2.9	11.0	99.3
24H-6, 62.5–64.5	225.32	238.85	60.73	21.3	6.8	8.8	96.3
24H-6, 67–69	225.37	240.40	60.98	7.0	5.3	2.7	95.6
24H-7, 121.5–123.5	225.91	240.95	61.02	7.5	3.5	14.1	96.4
24H-7, 17–19	226.37	241.40	61.04	15.0	12.4	3.8	89.8
24H-7, 35–37	226.55	241.58	61.05	10.9	4.2	5.7	94.7
24H-7, 52.5–54.5	226.73	241.76	61.06	19.4	19.8	3.5	93.1
25H-1, 68–70	226.88	241.91	61.06	4.9	3.7	6.4	96.4
25H-1, 35–37	227.05	243.33	61.13	10.2	6.2	5.5	90.5
25H-1, 50–52	227.20	243.48	61.13	4.4	3.1	9.3	93.0
25H-1, 65–67	227.35	243.63	61.14	10.3	6.3	4.2	87.3
25H-1, 82.5–84.5	227.52	243.81	61.15	1.3	2.1	8.2	93.8
25H-2, 100–102	227.70	243.98	61.15	5.6	13.3	1.5	92.8
25H-2, 17.5–19.5	228.38	244.66	61.18	6.4	6.3	6.3	94.3
25H-2, 32.5–34.5	228.52	244.81	61.19	18.1	22.4	1.7	91.9
25H-3, 75–77	228.95	245.23	61.33	5.3	6.6	7.6	93.2
25H-3, 7.5–9.5	229.77	246.06	61.80	9.6	18.9	0.8	90.1
25H-3, 47.5–49.5	230.18	246.46	62.02	18.2	48.7	0.7	95.1
25H-4, 115–117	230.85	247.13	62.41	7.9	16.7	0.7	83.0
25H-4, 70–72	231.90	248.18	63.00	0.7	1.4	15.8	96.0
25H-5, 130–132	232.50	248.78	63.35	0.7	0.0	24.0	96.5
25H-6, 85–87	233.55	249.83	64.13	0.9	0.8	27.9	97.3
25H-6, 10–12	234.30	250.58	64.69	0.7	0.0	24.8	84.7
25H-6, 90–92	235.10	251.38	64.92	0.3	0.5	31.5	94.5

Table T2. Sample, depths, age and dissolution indexes, Hole 1211A. (Continued on next page.)

Core, section, interval (cm)	Depth (mbsf)	Depth (mcd)	Age (Ma)	Fragment (%)	Benthic (%)	Coarse fraction (>38 µm) (wt%)	Carbonate content (wt%)
198-1211A-							
9H-6, 67–69	77.47	84.60	34.26	9.8	9.0	1.6	87.9
10H-1, 20–22	79.00	88.15	34.95	36.7	78.1	0.8	96.8
10H-1, 40–42	79.20	88.35	34.99	44.0	58.6	0.5	97.2
10H-1, 60–62	79.40	88.55	35.03	76.8	94.8	0.4	83.7
10H-1, 80–82	79.60	88.75	35.07	15.0	10.1	0.2	98.3
10H-1, 100–102	79.80	88.95	35.11	85.3	92.9	0.4	92.8
10H-1, 120–122	80.00	89.15	35.15	62.8	71.4	0.5	91.3
10H-1, 140–142	80.20	89.35	35.19	62.4	81.0	0.3	96.8
10H-2, 67–69	80.97	90.12	35.62	74.4	94.7	0.3	83.9
10H-3, 70–72	82.50	91.65	36.54	73.6	94.0	0.2	85.0
10H-4, 67–69	83.97	93.12	37.43	70.4	92.9	0.2	84.0
10H-5, 65–67	85.45	94.60	38.33	65.2	64.0	1.2	92.1
10H-6, 68–70	86.98	96.13	39.25	49.6	64.7	0.8	86.6
10H-7, 67–69	87.97	97.12	39.85	29.3	40.9	0.7	96.0
11H-1, 42–44	88.72	98.21	42.29	9.5	33.3	0.8	93.5
11H-1, 66–68	88.96	98.45	43.19	27.2	36.9	4.8	63.8
11H-2, 67–69	90.47	99.96	43.95	33.0	19.3		89.4
11H-3, 71.5–73.5	92.01	101.51	44.35	21.8	6.5	3.7	89.8
11H-4, 69–71	93.49	102.98	44.72	14.0	5.1	3.0	95.4
11H-4, 90–92	93.70	103.19	44.77	6.2	4.8	2.7	100.0
11H-5, 73–75	95.03	104.52	45.11	14.3	3.4	3.0	96.3
11H-6, 72–74	96.52	106.01	45.49	56.0	20.4		91.4
11H-7, 43–45	97.73	107.22	45.79	9.5	5.5	2.8	91.3
12H-1, 20–22	98.00	107.92	49.10	14.2	1.0	2.4	92.7
12H-1, 64–66	98.44	108.36	49.30	12.7	4.9	4.8	98.2
12H-2, 40.5–42.5	99.71	109.63	49.88	17.7	8.1	2.4	90.4
12H-2, 67–69	99.97	109.89	50.00	14.6	6.8	2.8	94.4
12H-2, 118–120	100.48	110.40	50.24	36.1	12.5	2.2	94.6
12H-3, 26.5–28.5	101.07	110.99	50.43	18.6	4.3	2.6	93.6
12H-3, 48–50	101.28	111.20	50.46	12.9	10.2	2.7	92.9
12H-3, 63–65	101.43	111.35	50.48	13.8	4.3	2.6	94.7
12H-3, 88–90	101.68	111.60	50.51	30.7	5.9	2.7	98.6
12H-3, 107–109	101.87	111.79	50.54	4.9	3.7	5.3	93.3
12H-3, 138–140	102.18	112.10	50.58	6.1	4.6	2.2	95.5
12H-4, 69–71	102.99	112.91	50.69	68.4	16.7	1.6	95.4
12H-4, 103–105	103.33	113.25	50.73	9.6	1.8	3.4	97.2
12H-4, 122–124	103.52	113.44	50.76	10.1	1.4	5.3	95.1
12H-5, 23–25	104.03	113.95	50.85	7.5	8.8	1.9	93.6
12H-5, 41–43	104.21	114.13	50.90	4.7	2.5	5.1	97.8
12H-5, 67–69	104.47	114.39	50.97	15.7	6.1	3.0	91.5
12H-5, 108–110	104.88	114.80	51.08	30.1	13.0	1.3	87.2
12H-5, 133–135	105.13	115.05	51.14	5.0	4.6	3.0	94.0
12H-6, 8–10	105.38	115.30	51.21	6.1	2.7	5.3	95.0
12H-6, 67–69	105.97	115.89	51.36	8.1	4.1		95.2
12H-6, 113–115	106.43	116.35	51.48	7.2	7.6	5.5	94.4
12H-7, 10–12	106.90	116.82	51.61	6.0	7.2	1.1	93.7
13H-1, 67–69	107.97	119.46	52.30	3.4	6.2	6.4	94.1
13H-1, 89–91	108.19	119.68	52.72	4.2	1.7	7.4	84.7
13H-2, 67–69	109.47	120.96	53.03	3.6	3.2	9.0	91.6
13H-3, 10–12	110.40	121.89	53.22	18.9	5.4	5.2	93.3
13H-3, 67–69	110.97	122.46	53.37	10.3	3.9	5.8	96.9
13H-3, 112.5–114.5	111.43	122.92	53.53	3.6	1.5	6.9	97.5
13H-4, 12–14	111.92	123.41	53.72	5.1	2.2	7.0	93.5
13H-4, 68–70	112.48	123.97	53.82	3.6	1.4		99.0
13H-4, 100–102	112.80	124.29	53.64	6.2	2.4	6.0	98.0
13H-5, 67–69	113.97	125.46	54.43	18.8	7.9	5.6	86.8
13H-5, 100–102	114.30	125.79	54.65	4.9	3.0	7.9	88.1
13H-6, 3–5	114.68	126.17	54.86	6.8	4.1	12.2	97.2
13H-6, 10–12	114.75	126.24	54.90	15.8	5.9	13.2	95.2
13H-6, 20–22	114.85	126.34	54.95	20.7	10.7	7.0	97.7
13H-6, 68–70	115.33	126.82	55.21	23.8	11.1	3.1	94.3
13H-7, 64–66	116.79	128.28	56.27	57.5	50.0	1.4	97.8
14H-1, 45.5–47.5	117.25	130.26	56.34	35.0	8.2	4.0	94.6
14H-1, 110–112	117.90	130.90	56.36	16.2	5.0	4.9	95.2
14H-2, 13–15	118.43	131.43	56.38	6.7	12.6	0.9	93.7

Table T2 (continued).

Core, section, interval (cm)	Depth		Age (Ma)	Fragment (%)	Benthic (%)	Coarse fraction (>38 µm) (wt%)	Carbonate content (wt%)
	(mbsf)	(mcd)					
14H-2, 67–69	118.97	131.97	56.39	54.4	37.3	1.3	98.4
14H-3, 21.5–23.5	120.01	133.02	56.43	50.2	37.0	1.5	95.5
14H-3, 67–69	120.47	133.47	56.45	11.2	2.2	5.1	94.0
14H-4, 65–67	121.95	134.95	56.50	7.5	2.1	7.8	99.1
14H-4, 96.5–98.5	122.26	135.27	56.72	8.7	2.2	7.3	93.8
14H-4, 118–120	122.48	135.48	56.97	14.2	7.5	6.0	90.8
14H-4, 138.5–140.5	122.68	135.69	57.21	23.6	10.9	4.7	93.0
14H-5, 21–23	123.01	136.01	57.58	41.6	16.7	4.4	94.1
14H-5, 42–44	123.22	136.22	57.83	45.1	24.0	1.5	93.7
14H-5, 60.5–62.5	123.40	136.41	58.04	86.0	93.5	0.6	89.9
14H-5, 67–69	123.47	136.47	58.12	11.1	8.3	2.2	88.9
14H-5, 80.5–82.5	123.61	136.61	58.27	42.0	80.0	0.6	88.8
14H-5, 96–98	123.76	136.76	58.45	88.4	97.6	0.5	93.1
14H-6, 5–7	124.35	137.35	59.10	61.8	66.7	2.0	85.0
14H-6, 16–18	124.46	137.46	59.11	37.2	56.8	0.5	92.5
14H-6, 66–69	124.96	137.96	59.14	38.4	12.4	0.6	98.7
14H-7, 42.5–44.5	126.22	139.23	59.21	27.0	8.1	5.7	90.3
14H-7, 59–61	126.39	139.39	59.22	44.3	46.7	0.7	94.2
15H-1, 23–25	126.53	141.79	59.37	5.9	3.9	6.2	95.5
15H-1, 43–45	126.73	141.99	59.38	6.8	4.7	8.1	97.4
15H-1, 90–92	127.20	142.46	59.50	3.7	0.0	13.3	92.5
15H-1, 130–132	127.60	142.86	59.82	11.4	7.4	6.2	97.7
15H-2, 36–38	128.16	143.42	60.23	13.6	16.4	3.3	92.6
15H-2, 67–69	128.47	143.73	60.43	7.3	2.1	8.5	97.5
15H-2, 93–95	128.73	143.99	60.61	22.4	16.7	2.6	92.4
15H-2, 133–135	129.13	144.39	60.87	26.5	16.2	2.6	100.0
15H-3, 23–25	129.53	144.79	61.06	7.3	12.2	4.1	92.8
15H-3, 98–100	130.28	145.54	61.59	1.0	0.0	27.8	94.3
15H-3, 130–132	130.60	145.86	62.18	1.2	0.0	20.8	90.3
15H-4, 28–30	131.08	146.34	63.14	0.9	0.0	30.9	95.6
15H-4, 58–60	131.38	146.64	64.36	0.0	0.0	39.3	96.2
15H-4, 95–97	131.75	147.01	64.78	0.1	0.0	40.4	97.7
15H-4, 118–120	131.98	147.24	64.83	0.0	0.0	33.3	99.2
15H-4, 140–142	132.20	147.46	64.88	0.7	1.0	17.7	93.1